The temporal evolution of magnesium isotope fractionation during hydromagnesite dissolution, precipitation, and at equilibrium

Eric H. Oelkers[1,2,*], Ulf-Niklas Berninger[1,3], Andrea Pérez-Fernàndez[1], Jérôme Chmeleff[1]

and Vasileios Mavromatis[1,4]

[1] Géosciences Environnement Toulouse, CNRS-UPS-OMP, 14 av. Édouard Belin, 31400 Toulouse, France.

[2] Department of Earth Sciences, UCL, Gower Street, WC1E 6BT London, United Kingdom.

[3] Department für Geo- und Umweltwissenschaften, LMU, Theresienstr. 41, 80333 München, Germany.

[4] Institute of Applied Geosciences, Graz University of Technology, Rechbauerstrasse 12, 8010 Graz, Austria

* Corresponding author e-mail: oelkers@get.omp.eu

Abstract- This study provides experimental evidence of the resetting of the magnesium (Mg) isotope signatures of hydromagnesite in the presence of an aqueous fluid during its congruent dissolution, precipitation, and at equilibrium at ambient temperatures over month-long timescales. All experiments were performed in batch reactors in aqueous sodium carbonate buffer solutions having a pH from 7.8 to 9.2. The fluid phase in all experiments attained bulk chemical equilibrium within analytical uncertainty with hydromagnesite within several days, but the experiments were allowed to continue for up to 575 days. During congruent hydromagnesite dissolution, the fluid first became enriched in isotopically light Mg compared to the dissolving hydromagnesite, but this Mg isotope composition became heavier after the fluid attained chemical equilibrium with the mineral. The δ^{26}Mg composition of the fluid was up to ~0.35 ‰ heavier than the initial dissolving hydromagnesite at the end of the dissolution experiments. Hydromagnesite precipitation was provoked during one experiment by increasing the reaction temperature from 4 to 50 ℃. The δ^{26}Mg composition of the fluid increased as hydromagnesite precipitated and continued to increase after the fluid attained bulk equilibrium with this phase. These observations are consistent with the hypothesis that mineral-fluid equilibrium is dynamic (i.e. dissolution and precipitation occur at equal, non-zero rates at equilibrium). Moreover the results presented in this study confirm 1) that the transfer of material from the solid to the fluid phase may not be conservative during stoichiometric dissolution, and 2) that the isotopic compositions of carbonate minerals can evolve even when the mineral is in bulk chemical equilibrium with its coexisting fluid. This latter observation suggests that the preservation of isotopic signatures of carbonate minerals in the geological record may require a combination of the isolation of fluid-mineral system from external chemical input and/or the existence of a yet to be defined dissolution/precipitation inhibition mechanism.

1. Introduction

The magnesium isotopic signatures preserved in the geologic record have been applied by the Earth Science community to characterize a plethora of natural processes and environments. For example, Mg isotopes have been used in an attempt to constrain Mg cycling in marine sediments (Higgins and Schrag, 2010), provide insight into past and present continental weathering processes (Pogge von Strandmann *et al.*, 2008; Pokrovsky *et al.*, 2011; Wimpenny *et al.*, 2011; Mavromatis *et al.*, 2014b), quantify carbonate diagenesis (Fantle and

Higgins, 2014), define ancient climatic events (Kasemann *et al.*, 2014), and as paleoenvironmental proxies (Pogge von Strandmann *et al.*, 2014; Geske *et al.,* 2015; Riechelmann et al., 2016). Critical to most of these applications is that magnesium isotopic ratios are preserved over significant and in some cases over geologic timeframes. The preservation of stable isotopic signatures in minerals, however, has been questioned by a number of studies in a variety of systems (e.g. Curti et al., 2010, Gorski and Fantle, 2017; Perez-Fernandez, 2017). For example, Pearce e*t al.* (2012) observed that Mg isotopic signatures continued to evolve between an aqueous fluid and coexisting magnesite at 150 and 200 °C after bulk chemical equilibrium was attained in this fluid − mineral system. Mavromatis *et al.* (2012) and Shirokova *et al.* (2013) observed a continuous re-equilibration of Mg isotopes between the hydrous Mg carbonate minerals nesquehonite and dypingite, and its co-existing aqueous fluid at ambient temperatures during experiments that lasted no more than 4 weeks. In a follow-up study, Mavromatis *et al.* (2015) reported the continuous re-equilibration of C isotopes between nesquehonite and dypingite and its co-existing aqueous fluid at the same conditions. Mavromatis *et al.* (2016b) reported the resetting of the Ba isotopic composition of witherite (BaCO$_3$) in contact with an aqueous fluid over the course of one week at 25 °C. The rapid exchange and resetting of Fe, Mn and O isotopic compositions have been reported during mineral-fluid reactions by Friedrdich et al. (2015, 2016). A significant number of observations also suggest that the divalent carbonate isotopic signatures can be reset in natural systems over geological timeframes (Fantle and DePaolo, 2007; Fantle *et al.*, 2010; Druhan *et al.*, 2013). Similar isotopic signature resetting was reported at ambient temperature during water-barite interaction by Curti *et al.* (2010), during water-epsomite interaction by Li *et al.* (2011), and during water-brucite interaction by Li *et al.* (2014). Building upon these past works, the present study provides further insight into the resetting of isotopic compositions though observations of the temporal evolution of Mg isotopic composition of fluids and coexisting hydromagnesite during its dissolution, precipitation, and at equilibrium.

This study is centered on the reactivity of hydromagnesite, a hydrous Mg-carbonate. Despite the fact that their formation is thermodynamically favored (Benezeth *et al.*, 2011), the formation of anhydrous Mg-carbonate minerals such as magnesite is unlikely to occur at ambient temperatures due to the strong hydration of aqueous magnesium (i.e. Lippmann, 1973; Saldi *et al.*, 2009, 2012; Mavromatis *et al.*, 2013; Gautier *et al.*, 2014). As such, hydrous magnesium carbonate minerals, such as hydromagnesite and nesquehonite are

relatively common in natural environments, where they occur as weathering products of mafic or ultramafic rocks (Deelman, 2011), within evaporate deposits (Alderman and Von de Borch, 1960; Goto *et al.,* 2003) and within speleotherms (Northup *et al.,* 2001). Hydromagnesite has also been observed to precipitate in microbial mats or stromatolites in a number of alkaline lakes (Power *et al.*, 2007, 2014; Shirokova *et al.*, 2011, 2013; Mavromatis *et al.*, 2012, 2015). The formation of these minerals can be catalyzed by bacterial activity (Thompson and Ferris, 1990; Power *et al.*, 2007, 2009, 2014; Shirokova *et al.*, 2013).

The formation of hydrous magnesium carbonates, such as hydromagnesite and nesquehonite has recently attracted interest due to their potential use in geological CO_2 storage, particularly at ambient temperature conditions where magnesite does not form (Teir *et al.,* 2009; King *et al.*, 2010; Hovelmann e*t al.,* 2012; Oskierski *et al.,* 2013; McCutcheon *et al.,* 2014, Power *et al.,* 2014). Notably, field observations have shown that passive CO_2 storage may occur in ultramafic mine tailings through the weathering of Mg-silicates and precipitation of hydrous Mg-carbonates (Wilson *et al.*, 2009, 2014; Pronost *et al.*, 2011). Such observations have motivated a number of experimental studies characterizing the formation conditions, reactivity, and thermal stability of the hydrous Mg-carbonates (Hänchen *et al.*, 2008; Frost *et al.*, 2008; Ballirano *et al.*, 2010; Gautier *et al.*, 2014; Berninger *et al.*, 2014). Other studies have investigated the mechanisms of hydromagnesite or nesquehonite formation during the carbonation of serpentine (Park and Fan, 2004; Teir *et al.*, 2007, 2009) and brucite (Zhao *et al.*, 2009; Schaef *et al.*, 2011; Loring *et al.*, 2012).

Numerous studies have focused on characterizing Mg isotope fractionation among anhydrous carbonate minerals and their co-existing fluids. For example, Mg isotope fractionation between fluids and co-existing magnesite and dolomite at elevated temperatures has been reported by Pearce *et al.* (2012) and Li *et al.* (2015), respectively. In each case, light Mg was found to be preferentially incorporated into to the solid phase. Corresponding fractionation has been measured for Mg in calcite at ambient temperatures (Li *et al.*, 2012; Mavromatis *et al.*, 2013; 2017a; 2017b). Work on Mg fractionation during hydrous Mg carbonate water interaction include that of Mavromatis *et al.* (2012) on dypingite at ambient temperatures and that of Shirokova *et al.* (2013) on the hydromagnesite stromatolites of Lake Salda, Turkey. These studies suggest that at equilibrium Mg in these hydromagnesite phases is ~1.0‰ lighter than their co-existing aqueous fluid phases. It should be emphasized, however, that the equilibrium distribution of Mg isotopes among minerals and their co-

existing aqueous fluids depends strongly on the fluid composition (Schott et al., 2016); the presence of substantial carbonate or aqueous organic species can alter these equilibrium fraction factors by up to several per mil. Due to these non-zero fractionation factors, the congruent dissolution of hydromagnesite could lead to an isotopic disequilibrium between the remaining hydromagnesite and an originally Mg-free fluid phase. This study takes advantage of this isotopic disequilibrium to assess how rapidly such Mg isotopic signatures may re-equilibrate isotopically with their co-existing fluid phase through a series of batch reactor experiments performed under strictly defined physicochemical conditions for up to 575 days.

A number of models have been proposed to describe the kinetically influenced evolution of carbonate mineral isotopic compositions during precipitation. The growth entrapment model, developed by Watson (1996; 2004), suggests the presence of a chemically and isotopically distinct surface layer that is in contact with the reactive fluid and can be either enriched or depleted in an isotopomer or a trace element. This model assumes that this reactive layer at the calcite surface is approximately 0.5 nm thick and has previously been applied to simulate uptake of elements and/or their isotopes in a number of experimental studies (*e.g.*, Mavromatis et al., 2013; 2015b; Noireaux et al., 2015; Gabitov et al., 2012; Tang et al., 2008a; 2008b; 2012). Alternatively, DePaolo (2011) developed a surface reaction kinetic model using the principle of transition state theory to simulate elemental and isotopic fractionation during calcite growth. In accord with transition state theory, this model is based on the two-way transfer of material to and from the mineral surface during its interaction with an aqueous fluid. It is assumed that removal of material from the mineral surface occurs with a distinct fraction factor from that of adding material to the surface. Similarly as mineral dissolution, like precipitation proceeds by the two-way transfer of material to and from the mineral surface, it seems likely that isotope fractionation will occur during dissolution, and continue as bulk chemical equilibrium is attained in the fluid-mineral system (c.g. Steefel et al., 2014). This study was designed to evaluate this possibility for the case of hydromagnesite.

2. Theoretical considerations

Isotope compositions in this paper are presented in delta notation, $\delta^{26}Mg$, corresponding to ratio of ^{26}Mg relative to ^{24}Mg normalized to the DSM3 standard (Galy *et al.,* 2003). The

isotopic offset between the metal in the solid and the fluid phase ($\Delta^{26}Mg_{solid-fluid}$) is defined by

$$\Delta^{26}Mg_{solid-fluid} = \delta^{26}Mg_{solid} - \delta^{26}Mg_{fluid} \qquad (1)$$

Note that all $\Delta^{26}Mg_{solid-fluid}$ values reported in this study are based on the average isotopic composition of the solids, which may be heterogeneous. The average isotopic composition of the solid phase during a closed system stoichiometric dissolution experiment can be calculated from the initial conditions of the reactor and the measured fluid phase isotopic composition from mass balance considerations taking account of (Criss, 1999)

$$\delta^{26}Mg_{total}m_{Mg,total} = \delta^{26}Mg_{solid}m_{Mg,solid} - \delta^{26}Mg_{fluid}m_{Mg,fluid} \qquad (2)$$

where $m_{Mg,solid}$ and $m_{Mg,fluid}$ refer to the mass of Mg in the solid and fluid phase, respectively. Note that the product $\delta^{26}Mg_{solid_{total}}m_{Mg,total}$ is constant during a closed system reactor experiment.

Within the context of transition state theory (e.g. Lasaga, 1981; Aagaard and Helgeson, 1982), mineral dissolution consists of two coupled processes, the removal of material from the mineral surface, sometimes referred to as the forward reaction (i.e. dissolution), and the inverse process, returning some of the dissolved material back to the mineral surface. This latter process can be referred to as the reverse reaction (i.e. precipitation). This latter reverse precipitation reaction is negligible in strongly undersaturated fluids, but becomes increasingly important as the fluid composition approaches equilibrium (Aagaard and Helgeson, 1982; Oelkers, 2001; Schott and Oelkers, 1995; Schott et al., 2009). At bulk chemical equilibrium, forward dissolution proceeds at an equal but opposite rate as the reverse precipitation reaction, such that the net reaction rate is zero. As such the non-conservative transfer of isotopes during the stoichiometric dissolution of a mineral and at mineral-fluid equilibrium can occur by the coupling of the conservative transfer of isotopologues of an element from the mineral to the fluid phase during forward dissolution to the fractionation of this element during it's reverse precipitation (see also DePaolo, 2011). The driving force for the non-conservative transfer of isotopes during stoichiometric dissolution and at bulk chemical equilibrium can stem from the isotopic disequilibrium caused by the forward dissolution of the mineral. The degree to which the mineral-fluid system attains an overall isotopic equilibrium, where the mineral is isotopically homogeneous and the

fluid has a composition consistent with the system's equilibrium fraction factor, will depend on the rate at which material brought back to the surface during reverse precipitation penetrates into the mineral. It should be emphasized that numerous studies have observed the exchange of one or more elements deep within the solids during congruent mineral or glass dissolution experiments (c.f. Casey et al., 1989; Chou and Wollast, 1989; Oelkers et al., 2009; Schott et al., 2012).

3. Methods

3.1 Thermodynamic calculations

The standard state adopted in this study for thermodynamic calculations is that of unit activity for pure minerals and H_2O at any temperature and pressure. For aqueous species other than H_2O, the standard state is unit activity of the species in a hypothetical 1 molal solution referenced to infinite dilution at any temperature and pressure. Hydromagnesite dissolution and precipitation can be described by the reaction:

$$Mg_5(CO_3)_4(OH)_2 \cdot 4H_2O \text{ (hydromagnesite)} + 6H^+ = 5Mg^{2+} + 4HCO_3^- + 6H_2O \qquad (3)$$

In accord with the standard state, the law of mass action for this reaction is given by:

$$K_{Hmgs} = \frac{a_{Mg^{2+}}^5 \; a_{HCO_3^-}^4}{a_{H^+}^6} \qquad (4)$$

where K_{Hmgs} stands for the equilibrium constant of the hydromagnesite hydrolysis reaction (3)

and a_i represents the activity of the subscripted aqueous species. The saturation state of the fluid phase with respect to hydromagnesite (Ω_{Hmgs}) can then be computed from

$$\Omega_{Hmgs} = \frac{a_{Mg^{2+}}^5 \; a_{HCO_3^-}^4}{K_{Hmgs} a_{H^+}^6} \qquad . \qquad (5)$$

All thermodynamic calculations in this study were performed using the PHREEQC (Version 2.18) computer code (Parkhurst and Appelo, 1999) together with its llnl database after adding the equilibrium constants for Mg^{2+} hydrolysis and the carbonic acid dissociation reported by Brown *et al.* (1996) and Millero *et al.* (2007), respectively, and the equilibrium constant for the hydromagnesite hydrolysis reaction and the solubility product of hydromagnesite reported by Gautier *et al.* (2014).

3.2 Experimental design

All experiments in this study were performed using natural hydromagnesite collected from stromatolite precipitates in Lake Salda in southwest Turkey. These solids and their sampling methods have been described by Shirokova *et al.* (2011, 2013). Prior to their use in the experiments, these solids were hand-milled with an agate mortar and pestle. The resulting powder was cleaned with 10% H_2O_2 to remove organics and oven dried at 50 ºC for 24 h. The particles were not cleaned ultrasonically due to the fine nature of these natural grains. Scanning Electron Microscope (SEM) images, obtained using a JEOL JSM-6360 LV microscope, of the resulting hydromagnesite are shown in Fig. 1. The hydromagnesite powder consists of agglomerated crystals; the agglomerates range up to 50 μm in size, and the size of the individual hydromagnesite crystals is ~5 μm. No other mineral phases were evident from SEM images nor were any detected using backscattered electron microscopy. The purity of this hydromagnesite, was verified via X-ray diffraction using an INEL CPS-120 diffractometer with Co Kα-radiation, $\lambda = 1.78897$ Å and a graphite monochromator. X-ray diffraction was performed from 1 to 110º 2θ at 0.09º/min. This analysis revealed no phase other than hydromagnesite. The surface area of the prepared hydromagnesite was determined to be 8.5 $m^2/g \pm 10\%$ according to the BET method (Brunauer *et al.*, 1938).

Two different types of batch experiments were performed in this study to illuminate the behavior of Mg fractionation during dissolution, precipitation and at equilibrium. Experiments Hmgs-1 Hmgs-3, Hmgs-4, and Hmgs-5 were single batch reactor experiments; the protocol for these experiments was presented in detail by Berninger *et al.* (2014). Experiment Hmgs-2 consisted of a series of 13 individual batch experiments; each ran for a selected elapsed time before being stopped. Experiments Hmgs-1, Hmgs-2, Hmgs-3, and Hmgs-4 were performed in 0.5 l high-density polypropylene reactors while experiment Hmgs-5 was performed in a 1 l high-density polypropylene reactor. Experiments Hmgs-1 to Hmgs-4 were initiated by placing ~1 g of hydromagnesite powder and 500 g of the initial reactive fluid into each reactor. Experiment Hmgs-5 was started by adding 10 g of hydromagnesite powder and 1 kg of initial reactive fluid to the reactor. The initial reactive fluids were composed of deionized H_2O and Merck reagent grade Na_2CO_3 and $NaHCO_3$, and had a pH of 7.7 to 9.2; the composition of all initial fluids is provided in Table 1. The Mg concentration of these initial fluids was below the analytical detection limit of our fluid analysis (see below). After filling with hydromagnesite and initial reactive fluids, the reactors were sealed and

placed into continuously shaken isothermal baths. Hydromagnesite was allowed to dissolve in the reactive fluids for up to 575 days. Fluids were sampled regularly from the traditional single batch reactors, and at the end of each individual batch reactor using Millipore 0.22 μm cellulose acetate syringe filters. Experiments Hmgs-3 and Hmgs-4 were not sampled for the first 170 days in an attempt to limit potential evaporation effects in these reactors. All but one experiment was maintained at 23 ±2.5 °C. The initial temperature during the final experiment (Hmgs-5) was set to 4 ±1 °C for the first 33 days then raised to 50 ±1 °C. Due to the retrograde solubility of hydromagnesite, increasing temperature lead the reactor fluid to be supersaturated with respect to this phase, provoking its precipitation. At the end of each experiment, the fluids were separated from solids using suction filtration through these 0.22 μm filters. The solids were oven dried at 50 °C for 24h then stored at ambient temperature prior to chemical and isotopic analyses. A subset of the fluid was used to measure pH and a second subset was first acidified with ultrapure HNO_3 then stored at 4 °C prior to further analysis.

3.3 Chemical analyses

Aqueous fluid magnesium concentrations of initial and samples fluids were measured by flame Atomic Absorption Spectroscopy (AAS) using a Perkin Elmer AAnalyst 400 with an uncertainty of ±2 % and a detection limit of 6×10^{-7} mol kg^{-1}. Alkalinity was determined following a standard HCl titration procedure using an automatic Schott TitroLine alpha TA10plus titrator with an uncertainty of ±1% and a detection limit of 5×10^{-7} eq kg^{-1}. Fluid pH was measured using a Metrohm 713 pH Meter combined electrode on the activity scale with NIST buffers (pH = 4.006, 6.865 and 9.183 at 25 °C). Solids were analyzed by SEM and X-ray diffraction (XRD) to verify their compositions following the experiments.

3.4 Mg isotope analyses

Prior to stable Mg isotope analyses, liquid and solid samples were chemically purified by cation exchange chromatography following a protocol similar to that reported earlier by (Mavromatis et al. 2012; 2013; Pearce et al. 2012; Shirokova et al. 2013). Fluid samples were evaporated to dryness and re-dissolved in aqueous 1M HNO_3 prior to loading onto columns for chromatographic separation. Hydromagnesite samples were dissolved in concentrated aqueous HNO_3 before being evaporated to dryness, and then dissolved again in aqueous 1M HNO_3. Aliquots of these solution samples were loaded onto 10 ml Bio-Rad poly-prop columns containing AG-50W-X12 resin (200–400 mesh) for separation of Mg^{2+} from Na^+.

Mg recovery after chromatographic separation was >99.5%. The Mg isotopes were measured with a Thermo-Finnigan 'Neptune' Multi Collector Inductively Coupled Plasma Mass Spectrometer (MC-ICP-MS) at the GET laboratory (Toulouse, France). All analyzed fluids were prepared in 0.3M HNO_3 and were introduced into the Ar plasma with a standard spray chamber. The instrumental mass fractionation effects were corrected via sample-standard bracketing using the DSM3 standard and all data are presented in delta notation values with respect to the DSM3. All sample analyses were run in triplicate, with the mean value being presented in the tables. All results are consistent with mass dependent fractionation. The reproducibility of the isotopic analyses was assessed by replicate of three Mg reference liquid standards (DSM3, CAM-1 and OUMg) and the dolomite carbonate standard JDo-1, yielding precisions better than 0.07‰; these measurements were in agreement with the previously published values (e.g. Bolou-Bi *et al.*, 2009; Wombacher *et al.*, 2009, Beinlich *et al.*, 2014; Mavromatis *et al.*, 2014a, b; 2016a).

4. Results

Representative photomicrographs of hydromagnesite recovered after the single batch experiments stopped after 30 minutes, 175 days, and 575 days as part of experimental series Hmgs-2 are shown in Fig. 1. Mass balance calculations, taking account of the measured Mg concentrations of the reactive fluids, indicate that as much as 12% of the hydromagnesite dissolved into the fluid phase during this experiment. Only hydromagnesite is evident in the images, consistent with the stoichiometric dissolution of this mineral; similarly XRD analysis of the solids following the experiments reveals only the presence of hydromagnesite. There is no evidence of hydromagnesite recrystallization at this scale, as the size of the individual crystals and the agglomerates recovered from these experiments appear to be similar to that of the initial hydromagnesite seed grains. The lack of secondary mineral precipitation is also consistent with geochemical calculations indicating that all secondary solids besides magnesite were undersaturated in the reactive fluids throughout the experiments. Note that the saturation indexes of the hydrous Mg carbonate minerals nesquehonite and dypinite were not calculated, as the equilibrium constants for their hydrolysis reactions are unavailable, though these minerals are less stable thermodynamically than hydromagnesite (Mavromatis et al., 2015).

The chemical and isotopic evolution of the reactive fluid during all experiments is presented in Table 2 and shown in Figs. 2 to 4. The Mg isotope composition of solid hydromagnesite used in the experimental is -1.1±0.1 ‰, which is identical to that reported for this hydromagnesite by Shirokova *et al.* (2011, 2013). Owing to the carbonate-rich reactive fluids, the alkalinity and pH remained close to constant during the experiments, other than in experiment Hmgs-1, during which the pH increased by ~0.9 units. This pH increase was due to the consumption of protons by the hydromagnesite dissolution reaction (3); the pH in the other experiments remained closer to constant because the pH of their initial reactive fluids was higher leading to aqueous CO_3^{2-} formation in the fluid phase as hydromagnesite dissolved. Chemical equilibrium between the fluid and the hydromagnesite is rapidly attained in all experiments consistent with the results reported by Berninger *et al.* (2014). For example, chemical equilibrium was attained after ~5 hours during experiment Hmgs-1 and after ~2 days during experiment Hmgs-2. Chemical equilibrium in this study is taken to be when the absolute value of saturation state of the fluid with respect to hydromagnesite is less than 0.1, which is a conservative estimate of the uncertainties in these saturation states. This difference in equilibration times of experiments Hmgs-1 and Hmgs-2 reflects the lower pH of the initial reactive fluid in the former experiment; carbonate mineral dissolution rates tend to decrease with increasing pH (Chou et al., 1989). The equilibration of the fluids required that ~12% and ~5% of the hydromagnesite dissolved during experiments Hmgs-1 and Hmgs-2, respectively. The difference in the mass dissolved to attain equilibrium in these experiments stems from the variation of hydromagnesite solubility as a function of pH. Notably, the isotopic composition of the fluid phase during these experiments evolves continuously and is distinct from that of the hydromagnesite seed crystals. During Hmgs-1, the $\delta^{26}Mg_{fluid}$ evolves from -1.0 ‰, consistent with the original seed material to -0.65 ‰ (see Fig. 2B); during Hmgs-2 the reactive fluid becomes initially enriched in ^{24}Mg, achieving a $\delta^{26}Mg_{fluid}$ of -1.33‰, but it is then progressively depleted in ^{24}Mg, achieving a $\delta^{26}Mg_{fluid}$ of -0.87±0.1 ‰ after only 16 days of reaction time (Fig. 3C). The reactive fluid continues to become more depleted in ^{24}Mg over time, attaining a $\delta^{26}Mg_{fluid}$ of -0.66±0.01 ‰ after 546 days of hydromagnestite-fluid interaction. Experiments Hmgs-3 and Hmgs-4 were performed using the same initial fluid and solids as Hmgs-2 but using a different experimental protocol to validate the results of Hmgs-2. These latter experiments produced a similar trend of increasing $\delta^{26}Mg_{fluid}$ with time, leading to a $\delta^{26}Mg_{fluid}$ of -0.72±0.02 ‰ after 575 days of reaction (Fig. 3C).

The evolution of the Mg concentration and isotopic composition of experiment Hmgs-5 is shown in Fig. 4. The reaction temperature of this experiment was 4 °C for the first 33 days. During this time the aqueous Mg concentration increased to 3.8×10^{-3} mol kg^{-1}, corresponding to the dissolution of ~3.7% of the original hydromagnesite seeds. During this time, the fluid became enriched in light Mg isotopes compared to the dissolving solid; the $\delta^{26}Mg_{fluid}$ was -1.3±0.1 ‰ after 33 days of dissolution compared to a $\delta^{26}Mg_{Hmgs}$ of -1.1‰ for the initial solid. After 33 days the reactor temperature was increased to 50 °C. The retrograde solubility leads to hydromagnesite precipitation and the decrease in fluid Mg concentration to less than 1×10^{-3} mol kg^{-1}. During this time the isotopic composition of the fluid became heavier than the original hydromagnesite attaining a value of $\delta^{26}Mg_{fluid}$ of -0.82±0.04‰ at approximately 300 days after the temperature increase. Note that the isotopic composition of Mg in the fluid phase continues to evolve after the fluid attained bulk chemical equilibrium with the precipitating hydromagnesite. Consistent with the small quantity of hydromagnesite dissolved, the Mg isotopic composition of the solid recovered from the reactor following this experiment is identical within uncertainty to that of the initial hydromagnesite powder.

5. Discussion

5.1 Temporal variation of reactive fluid Mg concentration and its approach to hydromagnesite equilibrium.

The reactive fluid aqueous Mg concentration during the closed system equilibrium dissolution and precipitation experiments performed in this study can be quantified using the hydromagnesite rate equation given by

$$r_{Hmgs} = ks\left(1 - \Omega_{Hmgs}\right)^{n} \tag{6}$$

where r_{Hmgs} stands for the rate of hydromagnesite dissolution, k refers to a rate constant, s designates the specific surface area of the hydromagnesite present in the reactor, n, signifies a reaction order, which is equal to 1/5 for hydromagnesite (Gautier et al., 2014), and Ω_{Hmgs} denotes the reactive fluid saturation state, as defined by Eqn. (5).

As there is not an analytical solution to Eqn. (6) and to account for the changing fluid-mineral ratio occurring due to sampling, it was numerically integrated to the data using an EXCEL spreadsheet and the parameter k adjusted to obtain the closest fit between calculated

and measured reactive fluid Mg concentrations as a function of time. These fits were performed assuming a constant hydromagnesite surface area equal to that measured prior to the experiments. The results of these fits are represented as dashed curves in Fig 2 to 4, and the values of k corresponding to these fits are provided in Table 3. Close matches between calculated and measured reactive fluid concentrations are evident. Although there is some uncertainty in fitting these fast reaction rates, they are consistent with the conclusions of Berninger et al. (2014), as precipitation rate constant was found to be substantially smaller than that of the dissolution rate constants.

5.2 *The temporal evolution of fluid and mineral Mg isotope compositions during stoichiometric hydromagnesite dissolution and at equilibrium*

The Mg isotopic composition of the fluid phase exhibits a complex behavior during hydromagnesite dissolution. The fluid phase of experiment Hmgs-2 becomes enriched in ^{24}Mg after 1.5 hours of elapsed time with the δ^{26}Mg$_{fluid}$ attaining a value of -1.33‰, which is about 0.2‰ lighter compared to the original hydromagnesite material (see Fig 3C). The δ^{26}Mg$_{fluid}$ approaches that of the original material within 6 days, and eventually becomes isotopically heavy compared to this original material. A similar temporal increase in δ^{26}Mg$_{fluid}$ is seen during experiment Hmgs-1. The δ^{26}Mg$_{fluid}$ of the first sample is identical within uncertainty to the original hydromagnesite seeds. The fluid then becomes progressively heavier and is about 0.3‰ heavier compared to the original hydromagnesite at the end of the experiment. No fluid phase samples were collected during the first 170 days of experiments Hmgs-3 and Hmgs-4, as they were designed to assess the long-term behavior of the studied water-hydromagnestie system. Nevertheless the Mg isotopic analyses of these experiments suggest the fluids may be becoming isotopically heavier with time between 170 and 600 days. Note that the temperature was measured to vary within the range of 23 ±2.5 °C; this slight variation did not appear to influence significantly either the chemical or isotopic evolution during the experiments. Similar to the fluid evolution during the initial part of the isothermal experiments, the fluid phase after 33 days of dissolution at 4 °C during experiment Hmgs-5 resulted in a fluid that was ~0.2 ‰ lighter than the dissolving solid.

The chemical and isotopic composition of the fluid phase during hydromagnesite dissolution presented above is consistent with two distinct processes. The first of these processes involved the initial preferential departure of light Mg from the hydromagnesite.

Such observations could be attributed to tendency for the lighter ^{24}Mg-O bonds to break relatively easier compared to the stronger ^{26}Mg-O bonds in the hydromagnesite structure (c.f. Hoefs, 1973; Criss, 1999). Note that at the initial stages of dissolution in the batch reactors adopted in this study, the fluid phase is strongly undersaturated, such that mass transfer is dominated by the net removal of Mg from the solid to the aqueous phase (e.g. the forward reaction dominates over the reverse reaction – see Aagaard and Helgeson, 1982; Oelkers *et al.*, 1994, 2001; Oelkers 2001; Schott and Oelkers, 1995; Schott *et al.*, 2009). As such, during the early stages of these experiments, the preferential initial release of light Mg is still evident in the fluid phase and negligible isotopic equilibration can occur by the return of material back to the hydromagnesite. Note that a similar initial release of isotopically light divalent metals to the aqueous phase has been observed during forsterite, basaltic glass, and pyrite dissolution (Verney-Caron et al., 2011; Oelkers et al., 2015; Maher et al., 2016; Wolfe et al., 2016). Some preferential departure of light Mg from hydromagnesite could arise from isotopic heterogeneity of the hydromagnesite used in the experiments. It seems likely that such effects are limited, however, as this mineral was ground prior to its use in the experiments, which will tend to homogenize the compositions of the mineral surfaces. Resolution of this possibility would require further experiments on demonstrably isotopically uniform hydromagnesite, perhaps prepared under carefully controlled conditions.

The second process that influences the Mg isotope composition of the reactive fluid during stoichiometric dissolution is the tendency for the fluid phase to become increasingly heavy after this initial stage of the experiment. The increase in δ^{26}Mg$_{fluid}$ at a constant total dissolved Mg concentration observed after the hydromagnesite-fluid system attained bulk chemical equilibrium requires ^{24}Mg to be reincorporated into and ^{26}Mg to be released from the mineral at equal but opposite quantities. This behavior is consistent with the concept of dynamic equilibrium (see above). At equilibrium the reverse reaction (e.g. reverse precipitation) equals that of the forward reaction (e.g. forward dissolution). The importance of the reverse precipitation reaction is such that the fluid-solid system can continue to evolve towards isotopic equilibrium even after bulk chemical equilibrium has been attained. This observation is consistent with the calculations reported by Steefel *et al.* (2014), which predicts the isotopic equilibration of a mineral-fluid system in the absence of bulk chemical disequilibrium based on a Transition-State Theory.

The equilibrium fractionation factor for Lake Salda hydromagnesite in aqueous fluids similar to those used in this study was reported to be $\Delta^{26/24}Mg_{solid-fluid}$ = -1.2 ‰ (Shirokova *et al.*, 2011, 2013; Mavromatis et al., 2012). Note that both experimental studies and field observations suggest that carbonate minerals tend to favor incorporation of lighter Mg into their structures (e.g. Immenhauser et al., 2010; Hippler et al., 2009; Mavromatis et al., 2013; 2017a; 2017b; Li et al., 2012; 2015; Geske et al., 2015; Riechelmann et al., 2016; Eisenhauer et al., 2009; Wombacher et al., 2011). The observed $\Delta^{26}Mg_{solid-fluid}$ at the end of Hmgs-1, Hmgs-2, Hmgs-3, and Hmgs-4 is only -0.3 to -0.4‰. There are two potential possible reasons why the observed fractionation at the end of our experiments are different from the equilibrium hydromagnesite-fluid fractionation factors reported by Shirokova *et al.* (2011, 2013) and Mavromatis et al. (2012). First, it is possible that equilibrium isotope fraction has yet to be attained in our experiments. Indeed, the Mg isotope composition of the fluid in experiments Hmgs-3 and Hmgs-4 appear to be increasing somewhat with time near the end of these experiments (see Fig. 3). The slow attainment of isotopic equilibrium when the system is at bulk fluid-mineral equilibrium could stem from the relatively slow migration of Mg within the mineral structure. The second possibility is that equilibrium fractionation was obtained in our experiments. Schott *et al.* (2016) reported that mineral-fluid Mg equilibrium fractionation factors can vary by more than 4‰ depending on the fluid composition. For example, according to Schott *et al.* (2016), the equilibrium fractionation factor for magnesium between a mineral its co-existing aqueous fluid $\Delta Mg_{mineral-fluid}$ is 4‰ lighter if Mg is present as Mg^{2+} rather than $MgHCO_3^o$. As such, a small difference in fluid composition could be responsible for the ~0.8‰ difference between the equilibrium fractionation factors reported by Shirokova *et al.* (2011, 2013) and Mavromatis et al. (2012), and the $\Delta^{26}Mg_{solid-fluid}$ values observed at the end of our 25 °C experiments (see below).

5.3 Isotopic evolution during hydromagnesite precipitation

The results of experiment Hmgs-5 demonstrate that the precipitation of hydromagnesite at 50 °C favors the incorporation of isotopically light Mg into the solid phase. The average composition of the precipitated hydromagnesite can be determined from mass balance considerations. Prior to the precipitation of hydromagnesite, the reactive fluid contained 3.8×10^{-3} mol kg^{-1} of Mg with a $\delta^{26}Mg_{fluid}$ of -1.35 ‰. After 45 days of precipitation, the reactive fluid contained 0.8×10^{-3} mol kg^{-1} of Mg with a $\delta^{26}Mg_{fluid}$ of -0.97 ‰. Mass balance, as calculated using Eqn. (2), requires that hydromagnesite precipitation removed 3.0

x 10^{-3} mol kg^{-1} of Mg having an average $\delta^{26}Mg_{Hmgs}$ of -1.45 ‰. A simple Rayleigh fraction model, if based on the one-way transfer from the fluid to the solid phase would require an average $\Delta^{26}Mg_{Hmgs-fluid}$ of -0.24 ‰ to reproduce the reactive fluid Mg isotope variation over this elapsed time. It should be noted, that after this time, the fluid Mg concentration remained constant indicating that hydromagnesite precipitation was complete, yet the $\delta^{26}Mg_{fluid}$ continued to evolve to lighter values with time. As such, it is not possible to deduce unambiguously an equilibrium fractionation factor from these observations. This suggests, however, that the equilibrium fractionation factor in this system is greater than the $\Delta^{26}Mg_{Hmgs-fluid}$ of -0.24 ‰ determined from the mass balance considerations described above. The conclusion that the isotopic fractionation during the rapid precipitation of hydromagnesite is smaller than its equilibrium value is consistent with the conclusions of Pearce et al. (2012) who noted that Mg fractionation decreases with increasing precipitation rates due to kinetic factors.

5.4 Preservation of isotopic signatures in natural systems

The results reported in this study illustrate that Mg isotopic compositions of hydromagnesite 1) are not be conservatively transferred to the fluid phase during its stoichiometric dissolution, and 2) can evolve towards isotopic equilibrium after bulk hydromgnesite-fluid equilibrium has been obtained in this system. These results are coherent with similar observations reported for other carbonate systems including Mg isotopic fractionation during the dissolution and precipitation of magnesite, nesquehonite, and dypingite (Pearce e*t al.*, 2012; Mavromatis *et al.*, 2012; Shirokova et al., 2013), and C isotope fractionation during nesquehonite and dypingite precipitation (Mavromatis *et al.*, 2015). Similar observations have also been reported for epsomite (Li *et al.*, 2011) and brucite (Li *et al.*, 2014). These studies all indicate that isotopic signatures continue to evolve towards an equilibrium state after bulk fluid-mineral equilibrium has been attained. Such observations appear to contravene the commonly held assumption that carbonate minerals can preserve their isotopic signatures of formation over geological timeframes. As such is seem likely that the preservation the original isotopic ratios of carbonate rocks in natural systems would require either the isolation of the carbonate mineral-fluid system from external chemical input, potentially by lowering rock permeability or a dramatic slowing of the coupled carbonate mineral dissolution/precipitation reactions at near to equilibrium conditions.

Turchyn and DePaolo (2011) suggested that such processes may play a role in isotopic preservation in some natural systems.

6. Conclusion

The results summarized above provide further evidence for the evolution of carbonate mineral isotopic signatures towards isotopic equilibrium in the presence of an aqueous phase at bulk chemical equilibrium conditions. This alteration of isotopic signatures can occur without any clear visual evidence of mineral recrystallization. Such observations suggest that the isotopic compositions of carbonate minerals recorded in the geological record should not be assumed to be fixed following their original precipitation, and may reflect at least some resetting during deposition and burial. The degree to which the isotopic signals are reset in carbonate minerals will depend on the relative mass of the mineral to the fluid phase and the degree to which this fluid phase is out of isotopic equilibrium with respect to its co-existing mineral. Similarly, as the isotopic composition of the fluid phase is clearly influenced by its interaction with its coexisting rocks over relatively short timeframes, it seems unlikely that flowing natural fluids preserve pristine records of the origin of these fluids.

References

Aagaard, P. and Helgeson, H.C., 1982. Thermodynamic and kinetic constraints on reaction-rates among minerals and aqueous solutions. 1. Theoretical considerations. *Am. J. Sci.* **282**, 237-285.

Aldermann, A.R. and Von der Borch, C.C. (1960) Occurrence of hydromagnesite in sediments of South Austrailia. *Nature,* 188, 931.

Ballirano, P., De Vito, C., Ferrini, V. and Mignardi, S., 2010. The thermal behavior and structural stability of nesquehonite, $MgCO_3 \times 3H_2O$, evaluated by in situ laboratory parallel-beam X-ray powder diffraction: New constraints on CO_2 sequestration within minerals. *J. Hazard. Mater.* **178**, 522–528.

Beinlich, A., Mavromatis, V., Austrheim, H. and Oelkers, E.H., 2014. Inter-mineral Mg isotope fractionation during hydrothermal ultramafic rock alteration – Implications for the global Mg-cycle. *Earth Planet. Sci. Lett.* **392**, 166-176.

Benezeth, P., Saldi, G.D., Dandurand, J.L. and Schott, J., 2011. Experimental determination of the solubility product of magnesite at 50 to 200 °C. *Chem. Geol.* **286**, 21-31.

Berninger, U.-N., Jordan, G., Schott, J. and Oelkers, E.H., 2014. The experimental determination of hydromagnesite precipitation rates at 22.5 to 75 °C. *Min. Mag.* **78**, 1405-1416.

Bolou-Bi, E.B., Vigier, N., Brenot, A. and Poszwa, A., 2009. Magnesium isotope compositions of natural reference materials. *Geostand. Geoanal. Res.* **33**, 95-109.

Brown, P.L., Drummond, S.E. and Palmer, D.A., 1996. Hydrolysis of magnesium (II) at elevated temperatures. *J. Chem. Soc.-Dalton Trans.* **1996**, 3071–3075.

Brunauer, S., Emmett, P.H. and Teller, E., 1938. Adsorption of gasses in multimolecular layers. *J. Am. Chem. Soc.* **60**, 309-319.

Casey, W.H., Westrich, H.R., Arnold, G.W. and Banfield, J.F., 1989. The surface chemistry of dissolving laboradorite feldspar. *Geochim. Cosmochim. Acta* **53**, 821-832.

Chou, L., Garrels, R.A. and Wollast, R., 1989. Comparative study of the kinetics and mechanism of dissolution of carbonate minerals. *Chem. Geol.* **78**, 269-282.

Chou L. and Wollast, R.,1989. Is the exchange reaction of alkali feldspars reversible? *Geochim. Cosmochim. Acta* **53**, 557-558.

Criss, R.E., 1999. Principles of stable isotope distribution. Oxford University Press.

Curti, E., Fujiwara, K., Iijima, K., Tits, J., Cuseta, C., Kitmura, A., Glaus, M.A. and Muller, W., 2010. Radium uptake during barite recrystallization at 23 ± 2°C as a function of solution composition: An experimental ^{133}Ba and ^{226}Ra tracer study. *Geochim. Cosmochim Acta* **74**, 3553-3570.

Deelman, J.C., 2011. Low temperature formation of magnesite and dolomite. Geology Series (2.3 ed.), Compact Disk Publications, Eindhoven, Then Netherlands.

DePaolo, D.J., 2011. Surface kinetic model for isotopic and trace element fractionation during precipitation of calcite from aqueous solutions. Geochim. Cosmochim. Acta 75, 1039-1056.

Druhan, J.L., Steefel, C.I., Williams, K.H. and DePaolo, D.J., 2013, Calcium isotope fractionation in groundwater: Molecular scale processes influencing field-scale behavior. *Geochim. Cosmochim. Acta* **119**, 93-116.

Eisenhauer, A., Kisakurek, B. and Bohm, F., 2009. Marine Calcification: An Alkaline Earth Metal Isotope Perspective. *Elements* **5**, 365-368.

Fantle, M.S. and DePaolo, D.J., 2007. Ca isotopes in carbonate sediment and pore fluid from ODP Site 807A: the Ca^{2+}(aq)-calcite equilibrium fractionation factor and calcite recrystallization rates in Pleistocene sediments. *Geochim. Cosmochim. Acta* **71**, 2524-2546.

Fantle, M.S. and Higgins, J. 2014. The effects of diagenesis and dolomitization on Ca and Mg isotopes in platform carbonates: Implications for the geochemical cycles of Ca and Mg. *Geochim. Cosmochi. Acta* **142**, 458-481.

Fantle, M.S., Maher K.M., and DePaolo D.J., 2010. Ca isotopic approaches for quantifying rates of marine burial diagenesis. Rev. Geophys. 48, RG302.

Frierdich, A.J., Spicuzza, M.J. and Scherer, M. M., 2016. Oxygen isotope evidence for Mn(II)-catalyzed recrystallization of manganite (γ-MnOOH). *Environ,. Sci. Tech.* **50,** 6374-6380.

Frierdich, A.J., Beard, B.L., Rosso, K.M., Scherer, M. M., Spicuzza, M.J., Valley, J.W. and Johnson, C.M., 2015. Low temperature non-stoichiometric oxygen-isotope exchange coupled to Fe(II)-goethite interactions,. *Geochim. Cosmochim Acta* **160,** 38-54.;

Frost, R.L., Bahfenne, S., Graham, J. and Martens, W.N., 2008. Thermal stability of artinite, dypingite and brugnatellite – Implications for the geosequestration of greenhouse gases. *Thermochim. Acta* **475**, 39–43.

Gabitov, R.I., Watson, E.B., Sadekov, A., 2012. Oxygen isotope fractionation between calcite and fluid as a function of growth rate and temperature: An in situ study. *Chem. Geol.* **306,** 92-102.

Galy, A., Yoffe, O., Janney, P.E., Williams, R.E., Cloquet, C., Alard, O., Halicz, L., Wadwha, A., Hutchen, I.D., Ramon, E. and Carignan, J., 2003. Magnesium isotopes heterogeneity of the isotopic standard SRM980 and new reference materials for magnesium-isotope-ratio measurements. *J. Anal. At. Spectrom.,* **18,** 1352-1356;

Gautier, Q., Bénézeth, P., Mavromatis, V. and Schott, J., 2014. Hydromagnesite solubility product and growth kinetics in aqueous solution from 25 to 75°C. *Geochim. Cosmochim. Acta* **138**, 1-20.

Geske A., Goldstein R.H., Mavromatis V., Richter D.K., Buhl D., Kluge T., John C.M., Immenhauser A. (2015) The magnesium isotope (δ^{26}Mg) signature of dolomites *Geochim. Cosmochim. Acta*, **149**, 131-151.

Gorski, C.A., and Fantle, M.S., 2017. Stable mineral recrystallization in low temperature aqueous systems: A critical review. *Geochim. Cosmochim. Acta,* **198,** 439-465.

Hänchen, M., Prigiobbe, V., Baciocchi, R. and Mazzotti, M., 2008. Precipitation in the Mg-carbonate system--effects of temperature and CO_2 pressure. *Chem. Eng. Sci.***63**, 1012-1028.

Hippler, D., Buhl, D., Witbaard, R., Richter, D.K. and Immenhauser, A., 2009. Towards a better understanding of magnesium-isotope ratios from marine skeletal carbonates. *Geochim. Cosmochim. Acta* **73**, 6134-6146.

Higgins, J.A. and Schrag, D.P., 2010. Constraining magnesium cycling in marine sediments using magnesium isotopes. *Geochim. Cosmochim. Acta* **74**, 5039-5053.

Hovelmann, J., Putnis, C.V., Ruiz-Agudo, E. and Austrheim, H. (2012) Direct nanoscale observations of CO_2 sequestration during brucite ($Mg(OH)_2$) dissolution. *Envir. Sci. Tech.,* **46,** 5353-5260.

Hoefs, J., 1973. *Stable isotope geochemistry*. Springer-Verlag, Berlin, 135pp.

Immenhauser, A., Buhl, D., Richter, D., Niedermayr, A., Riechelmann, D., Dietzel, M. and Schulte, U., 2010. Magnesium-isotope fractionation during low-Mg calcite precipitation in a limestone cave - Field study and experiments. *Geochim. Cosmochim. Acta* **74**, 4346-4364.

Kasemann, S.A., Pogge von Strandmann, P.A.E., Prave, A.R., Fallick, T.E., Elliott, T. and Hoffmann, K.-H., 2014. Continental weathering following Cryogenian glaciation: Evidence from calcium and magnesium isotopes. *Earth. Planet. Sci. Let.* **396**, 66-74.

King, H.E., Plumper, O. and Putnis, A. (2010) Effect of secondary phase formation of the carbonation of olivine. *Envir. Sci. Tech.* **44,** 6503-6509.

Lasaga, A.C., 1981. Transition state theory. *Rev. Min.* **8,** 135-168.

Li, W., Beard, B.L. and Johnson, C.M., 2011. Exchange and fractionation of Mg isotopes between epsomite and saturated $MgSO_4$ solution. *Geochim. Cosmochim. Acta* **75**, 1814-1824.

Li, W., Beard, B.L., Li, C., Xu, H. and Johnson, C.M., 2014. Magnesium isotope fractionation between brucite ($Mg(OH)_2$) and Mg aqueous species: Implications for silicate weathering and biogeochemical processes. *Earth Planet. Sci. Let.* **394**, 82-93.

Li, W., Beard, B.L., Li, C., Xu, H. and Johnson, C.M., 2015. Experimental calibration of Mg isotope fractionation between dolomite and aqueous solution and its geological implications. *Geochim. Cosmochim. Acta* **157**, 164-181.

Li, W., Chakraborty, S., Beard, B.L., Romanek, C.S. and Johnson, C.M., 2012. Magnesium isotope fractionation during precipitation of inorganic calcite under laboratory conditions. *Earth Planet. Sci. Lett.* **333-334**, 304-316.

Lippmann, F., 1973. *Sedimentary carbonate minerals*. Springer-Verlag, New York, 228pp.

Loring, J.S., Thompson, C.J., Zhang, C., Wang, Z., Schaef, H.T. and Rosso, K.M., 2012. In situ infrared spectroscopic study of brucite carbonation in dry to water-saturated supercritical carbon dioxide. *J. Phys. Chem.* **A 116**, 4768–4777.

Maher, K., Johnson, N.C., Jackson, A., Lammers, L.N., Torchinsky, A.B., Weaver, K.L., Bird, D.K. and Brown, G.E., 2016. A spatially resolved surface kinetic model for forsterite dissolution. *Geochim. Cosmochim. Acta* **174**, 313-334.

Mavromatis, V., Immenhauser, A., Buhl, D., Purgstaller, B., Baldermann, A. and Dietzel, M., 2017a. Effect of organic ligands on Mg partitioning and Mg isotope fractionation during low-temperature precipitation of calcite in the absence of growth rate effects. *Geochim. Cosmochim. Acta* **207**, 139-153.

Mavromatis, V., Purgstaller, B., Dietzel, M., Buhl, D., Immenhauser, A. and Schott, J., 2017b. Impact of amorphous precursor phases on magnesium isotope signatures of Mg-calcite. *Earth Planet. Sci. Lett.* **464**, 227-236.

Mavromatis, V., Rinder, T., Prokushkin, A.S., Pokrovsky, O.S., Korets, M.A., Chmeleff, J. and Oelkers, E.H., 2016a. The effect of permafrost, vegetation, and lithology on Mg and Si isotope composition of the Yenisey River and its tributaries at the end of the spring flood. *Geochim. Cosmochim. Acta* **191**, 32-46.

Mavromatis, V., van Zuilen, K., Purgstaller, B., Baldermann, A., Nägler, T.F. and Dietzel, M., 2016b. Barium isotope fractionation during witherite (BaCO$_3$) dissolution, precipitation and at equilibrium. *Geochim. Cosmochim. Acta* **190**, 72-84.

Mavromatis, V., Bundeleva, I.A., Shirokova, L.S., Millo, C., Pokrovsky, O.S., Bénézeth, P., Ader, M. and Oelkers, E.H., 2015. The continuous re-equilibration of carbon isotope compositions of hydrous Mg carbonates in the presence of cyanobacteria. *Chem. Geol.* **404**, 41-51.

Mavromatis, V., Gautier, Q., Bosc, O. and Schott, J., 2013. Kinetics of Mg partition and Mg stable isotope fractionation during its incorporation in calcite. *Geochim. Cosmochim. Acta* **114**, 188-203.

Mavromatis, V., Meister, P. and Oelkers, E.H., 2014a. Using stable Mg isotopes to distinguish dolomite formation mechanisms: A case study from the Peru Margin. *Chem. Geol.* **385**, 84-91.

Mavromatis, V., Pearce, C.R., Shirokova, L.S., Bundeleva, I.A., Pokrovsky, O.S., Benezeth, P. and Oelkers, E.H., 2012. Magnesium isotope fractionation during hydrous magnesium carbonate precipitation with and without cyanobacteria. *Geochim. Cosmochim. Acta* **76**, 161-174.

Mavromatis, V., Prokushkin, A.S., Pokrovsky, O.S., Viers, J. and Korets, M.A., 2014b. Magnesium isotopes in permafrost-dominated Central Siberian larch forest watersheds. *Geochim. Cosmochim. Acta* **147**, 76-89.

Millero, F., Huang, F., Graham, T. and Pierrot, D., 2007. The dissociation of carbonic acid in NaCl solutions as a function of concentration and temperature. *Geochim. Cosmochim. Acta* **71**, 46–55.

Noireaux, J., Mavromatis, V., Gaillardet, J., Schott, J., Montouillout, V., Louvat, P., Rollion-Bard, C., Neuville, D.R., 2015. Crystallographic control on the boron isotope paleo-pH proxy. *Earth Planet. Sci. Lett.* **430,** 398-407.

Northup, E., Kathleen, H. and Lavoie, D. (2001) Geomicrobiology of caves: A review. *Geomicrobio. J.* **18,** 199-222.

Oelkers, E.H., 2001. General kinetic description of multioxide silicate mineral and glass dissolution. *Geochim. Cosmochim, Acta* **65**, 3703-3719.

Oelkers, E.H., Benning, L.G., Lutz, S., Mavromatis, V., Pearce, C.R. and Plümper, O., 2015. The efficient long-term inhibition of forsterite dissolution by common soil bacteria and fungi at Earth surface conditions. *Geochim. Cosmochim. Acta* **168**, 222-235.

Oelkers, E.H., Golubev, S.V.,Chairat,C., Pokrovsky, O.S. and Schott, J., 2009. The surface chemistry of multi-oxide silicates. *Geochim. Cosmochim. Acta* **173**, 4617-4634.

Oelkers, E.H., Schott, J. and Devidal, J.-L., 1994. The effect of aluminum, pH, and chemical affinity on the rates of aluminosilicate dissolution reactions. *Geochim. Cosmochim. Acta* **58**, 2011-2024.

Oskierski, H.C., Dlugogorski, B.Z. and Jacobsen, G. (2013) Sequestration of atmospheric CO_2 in chrysotile mine tailings of the Woodsreef Asbestos Mine, Australia: Quantitative mineralogy, isotopic fingerprinting and carbonation rates. *Chem. Geo.* **358,** 156-169.

Park, A.H.A. and Fan, L.S., 2004. CO_2 mineral sequestration: physically activated dissolution of serpentine and pH swing process. *Chem. Eng. Sci.* **59**, 5241–5247.

Parkhurst, D.L. and Appelo, C.A.J., 1999. User's guide to PHREEQC (version 2) — a computer program for speciation, batch-reaction, one-dimensional transport, and inverse geochemical calculations. *U.S. Geological Survey Water-Resources Investigations Report* 99-4259 (310 pp.).

Pearce, C.R., Saldi, G.D., Schott, J. and Oelkers, E.H., 2012. Isotopic fractionation during congruent dissolution, precipitation and at equilibrium: Evidence from Mg isotopes. *Geochim. Cosmochim. Acta* **92**, 170-183.

Perez-Fernandez, A., Berninger, U.-N., Mavromatiz, V., P.A.E. Pogge Von Strandmann, and Oelkers, E.H., 2017. Ca and Mg isotope fractionation during the stoichiometric dissolution of dolomite at 51 to 126 °C and 5 bars CO_2 pressure. *Chem Geol.* **467,** 76-88.

Pogge von Strandmann, P.A.E., Burton, K.W., James, R.H., van Calsteren, P., Gislason, S.R. and Sigfusson, B., 2008. The influence of weathering processes on riverine magnesium isotopes in a basaltic terrain. *Earth Planet Sci. Let.* **276**, 187-197.

Pogge von Strandmann, P.A.E., Forshaw, J. and Schmidt, D.N., 2014. Modern and Cenozoic records of seawater magnesium from foraminiferal Mg isotopes. *Biogeosci.* **11**, 5155-5168.

Pokrovsky, B.G., Mavromatis, V. and Pokrovsky, O.S., 2011. Co-variation of Mg and C isotopes in late Precambrian carbonates of the Siberian platform: A new tool for tracing the change in weathering regime? *Chem. Geo.* **290**, 67-74.

Power, I.M., Wilson, S.A., Harrison, A.L., Dipple, G.M., McCutcheon, J., Southam, G. and Kenward, P.A., 2014. A depositional model for hydromagnesite-magnesite playas near Atlin, British Columbia, Canada. *Sedimentology* **61**, 1701-1733.

Power, I.M., Wilson, S.A., Thom, J.M., Dipple, G.M., Gabites, J.E. and Southam, G., 2009. The hydromagnesite playas of Atlin, British Columbia, Canada: A biogeochemical model for CO_2 sequestration. *Chem. Geol.* **260**, 286-300.

Power, I.M., Wilson, S.A., Thom, J.M., Dipple, G.M. and Southam, G., 2007. Biologically induced mineralization of dypingite by cyanobacteria from an alkaline wetland near Atlin, British Columbia, Canada. *Geochem. Trans.* **8**, 16.

Pronost, J., Beaudoin, G., Tremblay, J., Larachi, F., Duchesne, J., Hebert, R. and Constantin, M., 2011. Carbon sequestration kinetic and storage capacity of ultramafic mining waste. *Environ. Sci. Technol.* **45**, 9413–9420.

Saldi, G.D., Jordan, G., Schott, J. and Oelkers, E.H., 2009. Magnesite growth rates as a function of temperature and saturation state. *Geochim. Cosmochim. Acta* **73**, 5646-5657.

Saldi, G.D., Schott, J., Pokrovsky, O.S., Gautier, Q. and Oelkers, E.H., 2012. An experimental study of magnesite precipitation rates at neutral to alkaline conditions and 100-200°C as a function of pH, aqueous solution composition and chemical affinity. *Geochim. Cosmochim. Acta* **83**, 93-109.

Schaef, H.T., Windisch, C.F. and McGrail, B.P., 2011. Brucite [$Mg(OH_2)$] carbonation in wet supercritical CO_2: An in situ high pressure X-ray diffraction study. *Geochim. Cosmochim. Acta* **75**, 7458-7471.

Schott, J. and Oelkers, E.H., 1995. Dissolution and crystallization rates of silicate minerals as a function of chemical affinity. *Pure App. Chem.* **67**, 903-910.

Schott, J., Mavromatis, V., Fujii, T., Pearce, C.R. and Oelkers, E.H., 2016. The control of carbonate mineral Mg isotope composition by aqueous speciation: Theoretical and experimental modeling. *Chem. Geol.* **445**, 120-134.

Schott, J., Pokrovsky, O.S. and Oelkers, E.H., 2009. The link between mineral dissolution/precipitation kinetics and solution chemistry. *Rev. Min. Geochem.* **70**, 207-258.

Schott, J., Pokrovsky,O.S., Spalla, O., Devreux, F., Mielcarski, J.A., 2012. Formation,,growth and transformation of leached layers during silicate minerals dissolution: The example of wollastonite. *Geochim. Cosmochim. Acta* **98**, 259-281.

Shirokova, L.S., Mavromatis, V., Bundeleva, I.A., Pokrovsky, O.S., Benezeth, P., Gerard, E., Pearce, C.R. and Oelkers, E.H., 2013. Using Mg isotopes to trace cyanobacterially mediated magnesium carbonate precipitation in alkaline lakes. *Aquat. Geochem.* **19**, 1-24.

Shirokova, L.S., Mavromatis, V., Bundeleva, I.A., Pokrovsky, O.S., Benezeth, P., Pearce, C.R., Gerard, E., Balor, S. and Oelkers, E.H., 2011. Can Mg isotopes be used to trace cyanobacteria-mediated magnesium carbonate precipitation in alkaline lakes. *Biogeosciences Disc.* **8**, 6473-6517.

Steefel, C.I., Druhan, J.L. and Maher, K., 2014. Modelled coupled chemical and isotopic equilibration rates. *Proced. Earth Planet. Sci.* **10**, 208-217.

Tang, J., Dietzel, M., Böhm, F., Köhler, S.J., Eisenhauer, A., 2008a. Sr^{2+}/Ca^{2+} and $^{44}Ca/^{40}Ca$ fractionation during inorganic calcite formation: II. Ca isotopes. *Geochim. Cosmochim. Acta* **72**, 3733-3745.

Tang, J., Köhler, S.J., Dietzel, M., 2008b. Sr^{2+}/Ca^{2+} and $^{44}Ca/^{40}Ca$ fractionation during inorganic calcite formation: I. Sr incorporation. *Geochim. Cosmochim. Acta* **72**, 3718-3732.

Tang, J.W., Niedermayr, A., Köhler, S.J., Böhm, F., Kisakurek, B., Eisenhauer, A., Dietzel, M., 2012. Sr^{2+}/Ca^{2+} and $^{44}Ca/^{40}Ca$ fractionation during inorganic calcite formation: III. Impact of salinity/ionic strength. G*eochim. Cosmochim. Acta* 7**7**, 432-443.

Teir, S., Kuusik, R., Fogelholm, C.-J. and Zevenhoven, R., 2007. Production of magnesium carbonates from serpentinite for long-term storage of CO_2. *Int. J. Miner. Process.* **85**, 1–15.

Teir, S., Eloneva, S., Fogelholm, C.-J. and Zevenhoven, R., 2009. Fixation of carbon dioxide by producing hydromagnesite from serpentinite. *Appl. Energy* **86**, 214–218.

Thompson, J.P. and Ferris, F.G. (1990) Cyanobacerial precipitation of gypsum, calcite, and magnesite from natural alkaline water. *Geology* **18,** 995-998.

Turchyn, A.V. and DePaolo, D.J., 2011. Calcium isotope evidence for suppression of carbonate dissolution in carbonate-bearing organic-rich sediments. *Geochim. Cosmochim. Acta* **75**, 7081-7098.

Verney-Carron, A., Vigier, N., and Millot, R., 2011. Experimental determination of the role of diffusion on Li isotope glass weathering. *Geochim. Cosmochim.* Acta **75**, 3452-3468.

Watson, E.B., 1996. Surface enrichment and trace-element uptaking during crystal growth. *Geochim. Cosmochim. Acta* **60,** 5013-5020.

Watson, E.B., 2004. A conceptual model for near-surface kinetic controls on the trace-element and stable isotope composition of abiogenic calcite crystals. *Geochim. Cosmochim.* Acta **68**, 1473-1488.

Wilson, S.A., Dipple, G.M., Power, I.M., Thom, J.M., Anderson, R.G., Raudsepp, M., Gabites, J.E. and Southam, G., 2009. Carbon dioxide fixation within mine wastes of ultramafic-hosted ore deposits: Examples from the Clinton Creek and Cassiar chrysotile deposits, Canada. *Econ. Geol.* **104**, 95-112.

Wilson, S.A., Harrison, A. L., Dipple, G.M., Power, I.M., Barker, S.L.L., Mayer,K.U., Fallon, S.J., Raudsepp, M. and Southham, G. 2014. Offsetting CO_2 emissions by air capture in mine tailings

at the Mount Keith Nickel Mine, Western Australia: Rates, controls and prospects for carbon neutral; mining. *Int. J. Greenhouse Gas Cont.* **25**, 121-140.

Wimpenny, J., Burton, K.W., James, R., Gannoun, A., Mokadem, F. and Gislason, S.R., 2011. The behaviour of magnesium and its isotopes during glacial weathering in an ancient shield terrain in West Greenland. *Earth Planet. Sci. Let.* **304**, 260-269.

Wolfe, A.L., Stewart, B.W., Capo, R.C., Liu, R., Dzombak, D.A., Gordon, G.W., and Anbar, A.D., 2016. Iron isotope investigation of hydrothermal and sedimentary pyrite and their aqueous dissolution products. *Chem. Geol.,* **427,** 73-82.

Wombacher, F., Eisenhauer, A., Heuser, A. and Weyer, S., 2009. Separation of Mg, Ca and Fe from geological reference materials for stable isotope ratio analyses by MC-ICP-MS and double-spike TIMS. *J. Anal. At. Spectrom.* **24**, 627-636.

Wombacher, F., Eisenhauer, A., Böhm, F., Gussone, N., Regenberg, M., Dullo, W.C. and Rüggeberg, A., 2011. Magnesium stable isotope fractionation in marine biogenic calcite and aragonite. *Geochim. Cosmochim. Acta* **75**, 5797-5818.

Zhao, L., Sang, L., Chen, J., Ji, J. and Teng, H.H., 2009. Aqueous carbonation of natural brucite: relevance to CO_2 sequestration. *Environ. Sci. Technol.* **44**, 406–411.

Table 1: Initial conditions for all experiments run in this study.

| Experiment | hmgs seeds | composition of buffer solution | | pH | c$_{Mg}$ | Alkalinity |
	(g)	NaHCO$_3$ (g kg^{-1})	Na$_2$CO$_3$ (g kg^{-1})		(mol kg^{-1} x 10^{-6})	(eq/kg^{-1})
Hmgs-1	0.951	8.899[a]	0	7.77	7.79	0.105
Hmgs-2.1	1.000	6.973	0.848	9.02	5.13	0.096
Hmgs-2.2	1.001	6.973	0.848	9.02	5.13	0.096
Hmgs-2.3	0.999	6.973	0.848	9.02	5.13	0.096
Hmgs-2.4	1.000	6.973	0.848	9.02	5.13	0.096
Hmgs-2.5	0.999	6.973	0.848	9.02	5.13	0.096
Hmgs-2.6	1.000	6.973	0.848	9.02	5.13	0.096
Hmgs-2.7	0.999	6.973	0.848	9.02	5.13	0.096
Hmgs-2.8	1.000	6.973	0.848	9.22	6.35	0.098
Hmgs-2.9	1.002	6.973	0.848	9.22	6.35	0.098
Hmgs-2.10	1.000	6.973	0.848	9.22	6.35	0.098
Hmgs-2.11	1.001	6.973	0.848	9.22	6.35	0.098
Hmgs-2.12	1.000	6.973	0.848	9.22	6.35	0.098
Hmgs-2.13	1.001	6.973	0.848	9.22	6.35	0.098
Hmgs-3	0.999	6.973	0.848	9.22	6.35	0.098
Hmgs-4	1.001	6.973	0.848	9.22	6.35	0.098
Hmgs-5	10.00	6.973	0.848	9.02	5.13	0.096

[a] In addition, 4.9 mL of 1N HCl was added to this initial reactive fluid.

Table 2: Summary of experimental data

Experiment /sample	Time (days)	T (°C)	pH	c_{Mg} (mol kg^{-1} x 10^{-3})	alkalinity (eq kg^{-1})	δ^{25}Mg	sd	δ^{26}Mg	sd	Ω_{Hmgs}	aMg^{2+} / aCO$_3^{2-}$	Fluid mass (g)	%Mg in fluid
Hmgs-1.1	0.01	22.5	8.34	2.87	0.109	-0.51	0.04	-1.01	0.07	-3.19	1.02	499.99	6.0
Hmgs-1.2	0.02	22.5	8.43	3.89	0.110					-2.06	1.08	494.58	8.1
Hmgs-1.3	0.04	22.5	8.47	4.24	0.111					-1.72	1.06	490.20	8.7
Hmgs-1.4	0.06	22.5	8.51	5.07	0.113	-0.38	0.05	-0.77	0.01	-1.14	1.12	486.09	10.3
Hmgs-1.5	0.12	22.5	8.56	5.46	0.113					-0.72	1.06	481.75	11.0
Hmgs-1.6	0.16	23.0	8.58	5.90	0.114	-0.40	0.02	-0.78	0.03	-0.45	1.06	477.46	11.8
Hmgs-1.8	0.27	23.0	8.63	5.96	0.114					-0.23	0.94	470.39	11.8
Hmgs-1.9	0.32	23.0	8.65	6.01	0.115					-0.10	0.89	467.72	11.8
Hmgs-1.10	0.47	23.0	8.64	6.29	0.115					-0.07	0.96	465.26	12.3
Hmgs-1.12	1.29	23.0	8.70	5.71	0.115	-0.40	0.02	-0.79	0.02	0.01	0.74	459.19	11.0
Hmgs-1.13	1.91	22.0	8.71	5.30	0.113					-0.12	0.70	456.85	10.2
Hmgs-1.14	2.36	23.0	8.71	5.25	0.114					-0.13	0.66	453.80	10.0
Hmgs-1.15	2.92	22.5	8.71	5.61	0.114	-0.33	0.01	-0.65	0.03	-0.01	0.72	451.21	10.6
Hmgs-1.17	4.17	22.5	8.75	5.20	0.114	-0.41	0.07	-0.79	0.03	0.0	0.60	445.88	9.7
Hmgs-2.1	0.03	25.5	9.04	0.92	0.098	-0.60	0.04	-1.22	0.06	-2.34	0.05	539.82	2.0
Hmgs-2.2	0.07	25.5	9.05	1.16	0.098	-0.67	0.04	-1.33	0.04	-1.84	0.06	542.05	2.5
Hmgs-2.3	0.28	25.5	9.05	1.55	0.098	-0.48	0.05	-0.94	0.05	-1.17	0.09	538.66	3.3
Hmgs-2.4	0.99	25.5	9.09	1.93	0.098	-0.57	0.03	-1.19	0.02	-0.56	0.10	540.99	4.2
Hmgs-2.5	6.81	24.0	9.13	2.31	0.100	-0.52	0.03	-1.06	0.06	-0.04	0.11	538.56	5.0
Hmgs-2.6	16.22	25.0	9.17	2.23	0.103	-0.42	0.04	-0.87	0.04	0.01	0.09	542.65	4.8
Hmgs-2.7	33.14	24.5	9.09	2.18	0.103					-0.32	0.11	534.84	4.6
Hmgs-2.8	174.63	21.0	9.09	2.39	0.103	-0.37	0.02	-0.72	0.05	-0.10	0.13	540.38	5.2

Hmgs-2.9	205.48	21.5	9.15	2.28	0.102					0.01	0.10	540.78	4.9
Hmgs-2.10	239.87	21.5	9.17	2.25	0.103					0.03	0.10	540.83	4.9
Hmgs-2.11	359.78	23.5	9.20	2.03	0.103	-0.37	0.03	-0.70	0.03	-0.10	0.08	540.64	4.4
Hmgs-2.12	490.71	21.0	9.20	2.12	0.103					-0.01	0.09	541.00	4.6
Hmgs-2.13	545.65	21.5	9.15	2.08	0.102	-0.33	0.02	-0.67	0.01	-0.20	0.10	540.38	4.5
Hmgs-3.1	174.63	21.0	9.09	2.40	0.102	-0.49	0.02	-0.97	0.02	-0.09	0.13	540.29	5.2
Hmgs-3.2	205.49	21.5	9.15	2.28	0.102					0.01	0.11	533.63	4.9
Hmgs-3.3	239.87	21.5	9.16	2.21	0.102	-0.47	0.02	-0.94	0.03	-0.05	0.10	527.34	4.6
Hmgs-3.4	359.78	23.5	9.20	2.04	0.100	-0.45	0.02	-0.92	0.03	-0.09	0.08	520.99	4.2
Hmgs-3.5	490.73	21.0	9.18	2.10	0.101					-0.09	0.09	514.54	4.3
Hmgs-3.6	545.66	21.5	9.16	2.07	0.102					-0.17	0.09	507.83	4.2
Hmgs-3.7	574.71	24.0	9.16	2.13	0.102					-0.10	0.09	501.40	4.3
Hmgs-4.1	174.63	21.0	9.09	2.40	0.102	-0.49	0.03	-0.98	0.06	-0.10	0.13	540.19	5.2
Hmgs-4.2	205.50	21.5	9.15	2.28	0.102					-0.04	0.11	533.46	4.9
Hmgs-4.3	239.87	21.5	9.17	2.21	0.102					-0.02	0.10	526.95	4.6
Hmgs-4.4	359.78	23.5	9.21	2.04	0.101	-0.45	0.01	-0.92	0.03	-0.07	0.08	520.65	4.2
Hmgs-4.5	490.73	21.0	9.19	2.10	0.102					-0.06	0.09	514.11	4.3
Hmgs-4.6	545.65	21.5	9.16	2.07	0.102					-0.18	0.09	507.29	4.2
Hmgs-4.7	574.71	24.0	9.16	2.16	0.103	-0.36	0.01	-0.72	0.02	-0.09	0.09	500.80	4.3
Hmgs-5.1	8.01	4.0	9.30	3.31	0.099					-0.68	0.21	1181.82	1.6
Hmgs-5.2	14.04	4.0	9.41	3.38	0.102					-0.63	0.16	1175.55	1.6
Hmgs-5.3	22.07	4.0	9.48	3.49	0.103					-0.38	0.14	1169.70	1.6
Hmgs-5.4	32.89	4.0 / 50.0	9.30 / 8.89	3.79	0.103	-0.68	0.13	-1.32	0.13	-0.32 / 2977.8	0.23 / 0.16	1163.57	1.8
Hmgs-5.5	38.68	50.0	8.92	2.15	0.100	-0.52	0.15	-1.02	0.15	1.87	0.09	1157.73	1.0
Hmgs-5.6	49.60	50.0	9.02	0.86	0.098	-0.21	0.02	-0.47	0.04	0.19	0.03	1151.64	0.4

Hmgs-5.7	57.80	50.0	8.90	0.79	0.097					0.20	0.03 1145.76	0.4
Hmgs-5.8	63.55	50.0	8.94	0.80	0.098					0.15	0.03 1139.52	0.4
Hmgs-5.9	71.75	50.0	9.04	0.80	0.098					0.11	0.02 1133.45	0.4
Hmgs-5.10	78.76	50.0	9.01	0.79	0.097	-0.48	0.06	-0.97	0.06	0.04	0.03 1127.48	0.4
Hmgs-5.11	133.12	50.0	9.10	0.92	0.096	-0.43	0.05	-0.82	0.11	0.01	0.02 1121.38	0.4
Hmgs-5.12	307.79	50.0	8.98	0.68	0.098	-0.43	0.04	-0.82	0.04	0.10	0.02 1113.72	0.3
Hmgs-5.13	316.63	50.0	9.06	0.75	0.100					0.03	0.02 1101.80	0.3

Experiment	k (mol m^{-2} s^{-1})
Hmgs-1	6x10^{-6}
Hmgs-2, Hgms-3, Hmgs-4	4x10^{-7}
Hmgs-5	2x10^{-9}

Table 3. Summary of rate constants used to describe the temporal evolution of aqueous Mg concentrations during all experiments using Eqn. (6).

FIGURE CAPTIONS

Figure 1. Scanning Electron Micrographs of (A) the initial hydromagnesite seed material, (B) after the dissolution experiments Hmgs-2.1, (C) after dissolution experiment Hmgs-2.8, and (D) after dissolution experiment Hmgs-4.7. No change in morphology or grain size is observed during the experiments.

Figure 2. Temporal evolution of reactive fluid A) aqueous Mg concentration and B) Mg isotopic composition during batch reactor experiment Hmgs-1. Uncertainties in the concentration measurements are within the size of the symbols. Note that near constant aqueous Mg concentrations are attained in ~1 hour. The curves through the data in figure 2A were generated from a fit using Eqn. (6) together with the parameters provided in Table 3. The line in Fig 2B and the grey shaded area correspond to the Mg isotopic composition of the original hydromagnesite and its associated uncertainty, respectively.

**Figure 3.** Temporal evolution of A) aqueous Mg concentration during the first 16 days of individual batch reactor experiments Hmgs-2, B) the temporal evolution of the Mg isotopic compositions of these reactive fluid during this experiment, C) Mg concentration during experiments Hmgs-2, Hmgs-3, and Hmgs-4, and D) the isotopic composition during the these experiments. The open circles and triangles correspond to the results of experiment Hmgs-2 and experiments Hmgs-3 and Hmgs4, respectively. The curves through the data in figures 3A and 3C were generated from a fit using Eqn. (6) together with the parameters provided in Table 3. The line in Figs 3B and 3D and the grey shaded area correspond to the Mg isotopic composition of the original hydromagnesite and its associated uncertainty, respectively.

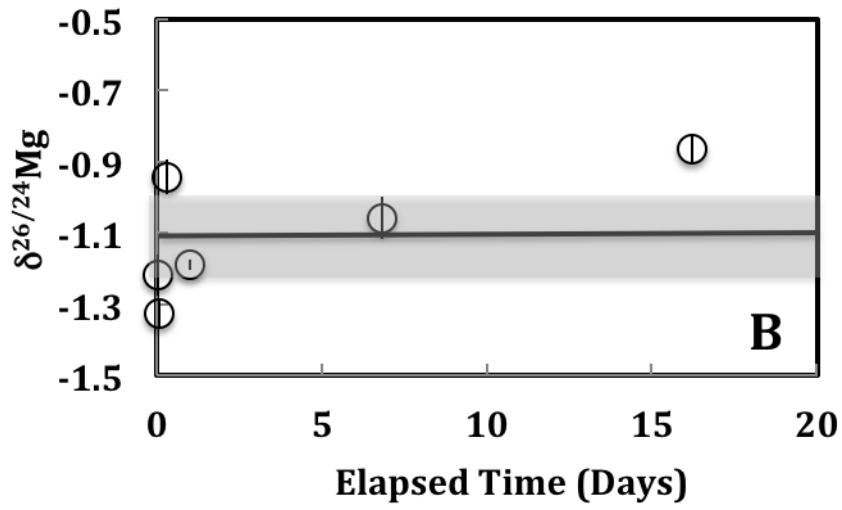**Figure 4.** Temporal evolution of aqueous Mg concentration and isotopic composition during experiment Hmgs-5. Note that the reactor temperature was increased from 4 to 50°C at day 33 provoking hydromagnesite precipitation; this time is indicated by the vertical line. The curves through the data in figure 4A were generated from a fit using Eqn. (6) together with the parameters provided in Table 3. The line and the grey shaded area in Fig 3B correspond to the Mg isotopic composition of the original hydromagnesite and its associated uncertainty, respectively.
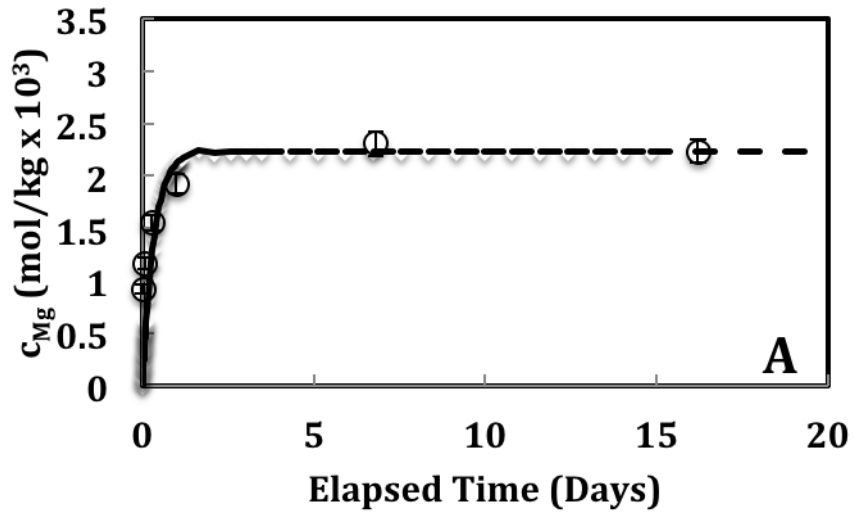
.

Figure 1
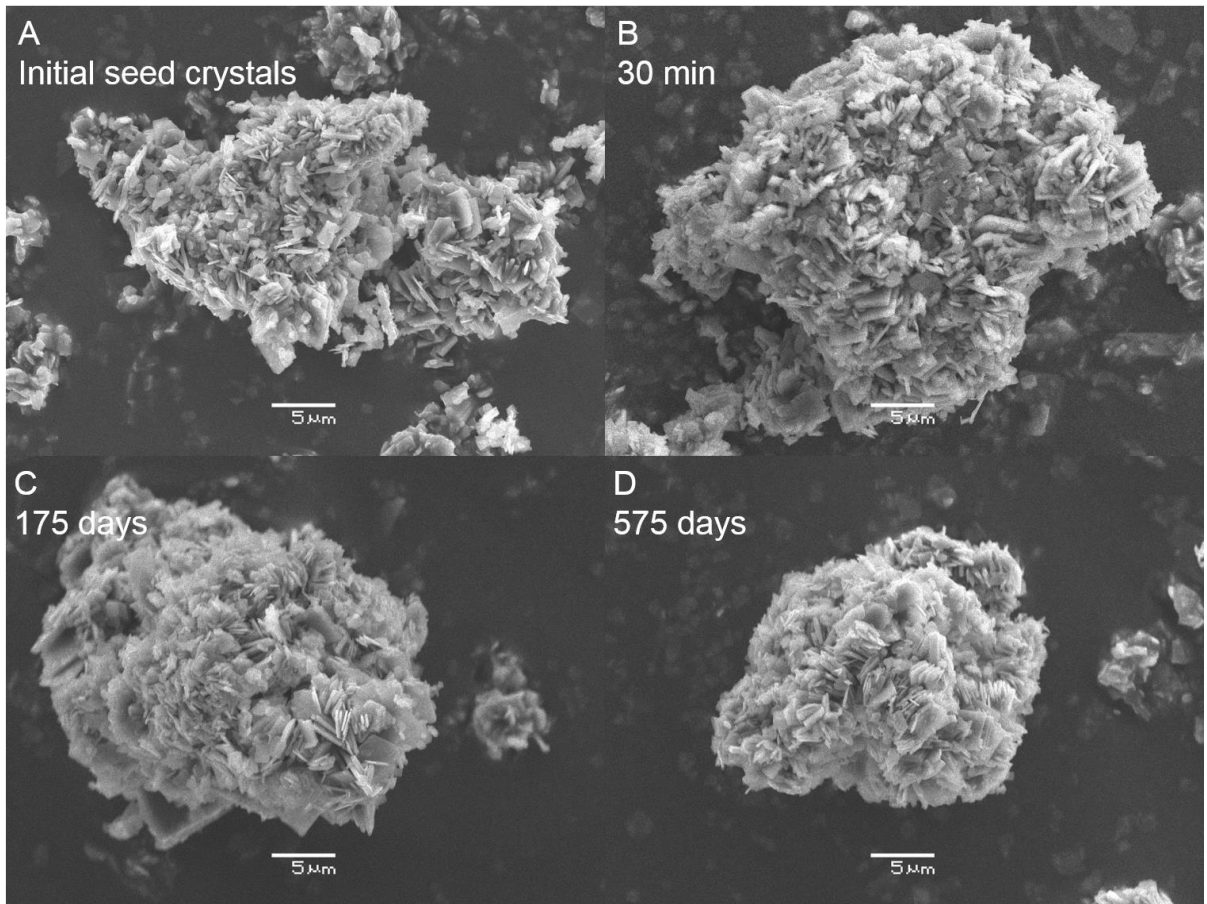
Figure 2
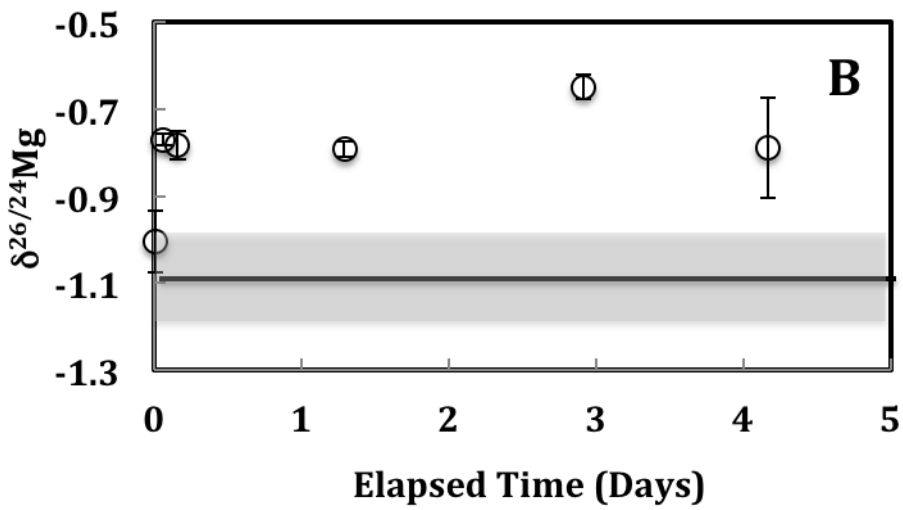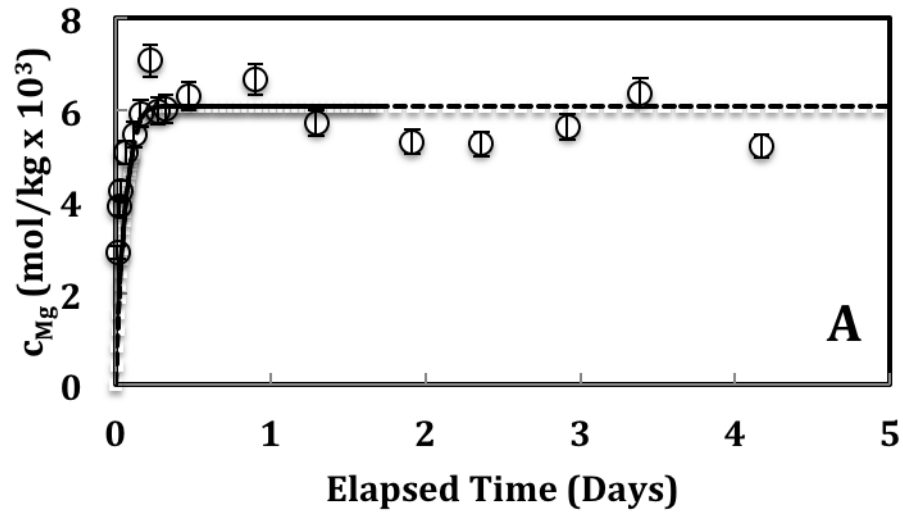
Figure 3

Figure 3 (continued)

Figure 4